Meteoritics & Planetary Science 40, Nr 2, 239–253 (2005)
Abstract available online at http://meteoritics.org

The formation of the Widmanstätten structure in meteorites

J. YANG* and J. I. GOLDSTEIN

Department of Mechanical and Industrial Engineering, College of Engineering, University of Massachusetts, Amherst, Massachusetts 01003, USA
*Corresponding author. E-mail: jiyang@ecs.umass.edu

(Received 16 October 2003; revision accepted 13 November 2004)

Abstract–We have evaluated various mechanisms proposed for the formation of the Widmanstätten pattern in iron meteorites and propose a new mechanism for low P meteoritic metal. These mechanisms can also be used to explain how the metallic microstructures developed in chondrites and stony-iron meteorites.

The Widmanstätten pattern in high P iron meteorites forms when meteorites enter the three-phase field $\alpha + \gamma + Ph$ via cooling from the $\gamma + Ph$ field. The Widmanstätten pattern in low P iron meteorites forms either at a temperature below the $(\alpha + \gamma)/(\alpha + \gamma + Ph)$ boundary or by the decomposition of martensite below the martensite start temperature. The reaction $\gamma \rightarrow \alpha + \gamma$, which is normally assumed to control the formation of the Widmanstätten pattern, is not applicable to the metal in meteorites. The formation of the Widmanstätten pattern in the vast majority of low P iron meteorites (which belong to chemical groups IAB–IIICD, IIIAB, and IVA) is controlled by mechanisms involving the formation of martensite α_2. We propose that the Widmanstätten structure in these meteorites forms by the reaction $\gamma \rightarrow \alpha_2 + \gamma \rightarrow \alpha + \gamma$, in which α_2 decomposes to the equilibrium α and γ phases during the cooling process.

To determine the cooling rate of an individual iron meteorite, the appropriate formation mechanism for the Widmanstätten pattern must first be established. Depending on the Ni and P content of the meteorite, the kamacite nucleation temperature can be determined from either the $(\gamma + Ph)/(\alpha + \gamma + Ph)$ boundary, the $(\alpha + \gamma)/(\alpha + \gamma + Ph)$ boundary, or the M_s temperature. With the introduction of these three mechanisms and the specific phase boundaries and the temperatures where transformations occur, it is no longer necessary to invoke arbitrary amounts of under-cooling in the calculation of the cooling rate.

We conclude that martensite decomposition via the reactions $\gamma \rightarrow \alpha_2 \rightarrow \alpha + \gamma$ and $\gamma \rightarrow \alpha_2 + \gamma \rightarrow \alpha + \gamma$ are responsible for the formation of plessite in irons and the metal phases of mesosiderites, chondrites, and pallasites. The hexahedrites (low P members of chemical group IIAB) formed by the massive transformation through the reaction $\gamma \rightarrow \alpha_m \rightarrow \alpha$ at relatively high temperature in the two-phase $\alpha + \gamma$ region of the Fe-Ni-P phase diagram near the $\alpha/(\alpha + \gamma)$ phase boundary.

INTRODUCTION

The Widmanstätten pattern in meteorites develops as a two-phase intergrowth of kamacite (α-bcc, ferrite) and taenite (γ-fcc, austenite). The Widmanstätten pattern is thought to form by the nucleation and growth of kamacite from taenite during slow cooling of the parent meteorite body (Owen and Burns 1939). The conventional explanation of the formation of the Widmanstätten pattern in meteorites is based on the binary Fe-Ni equilibrium phase diagram (Fig. 1; Yang et al. 1996). However, there is ample evidence from cooling experiments using Fe-Ni alloys that it is not possible to nucleate α phase in single crystal γ phase before forming the martensite α_2 phase (Allen and Earley 1950; Narayan and Goldstein 1984; Reisener and Goldstein 2003a). In fact, Reisener and Goldstein (2003a) showed that the only way for α to form in Fe-Ni alloys during cooling is by nucleation at grain boundaries.

Experimental studies have shown that phosphorus, which is present up to 2 wt% in iron meteorites (Buchwald 1975), has a significant influence on the development of the Widmanstätten pattern (Goldstein and Doan 1972). The presence of P changes the $\alpha/(\alpha + \gamma)$ and $\gamma/(\alpha + \gamma)$ phase boundaries in the Fe-Ni phase diagram (Buchwald 1966; Doan and Goldstein 1970; Romig and Goldstein 1980, 1981a) and affects the nucleation and growth mechanisms of the

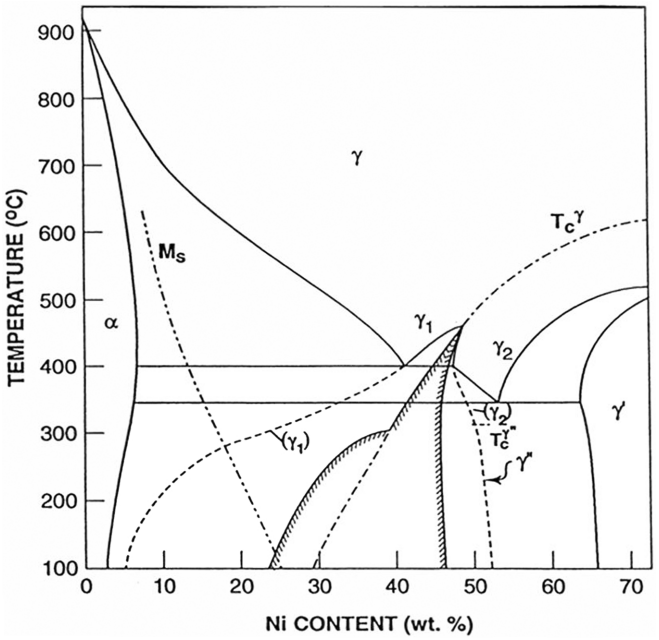

Fig. 1. Fe-Ni binary phase diagram (Yang et al. 1996): α is low Ni bcc phase; γ is a high Ni fcc phase; γ_1 is a low Ni paramagnetic fcc phase; γ_2 is a high Ni ferromagnetic fcc phase; γ′ is ordered Ni_3Fe; γ″ is ordered FeNi-tetrataenite; and M_s is the martensite starting temperature. T_c^{γ} is the Curie temperature of the γ phase. $T_c^{\gamma''}$ is the ordering temperature of FeNi, γ″.

Widmanstätten pattern (Goldstein and Doan 1972; Narayan and Goldstein 1984; Reisener and Goldstein 2003a).

Several experimental studies (Goldstein and Doan 1972; Narayan and Goldstein 1984; Reisener and Goldstein 2003a) have shown that kamacite α nucleates from single crystal taenite (γ phase) in high-P-bearing Fe-Ni alloys during cooling (i.e., an alloy containing 0.3 wt% P, 9.8 wt% Ni; Goldstein and Doan 1972). On the other hand, α does not nucleate from single crystal taenite γ in low-P-bearing Fe-Ni alloys (i.e., an alloy containing 0.15 wt% P, 9.06 wt% Ni; Narayan and Goldstein 1984). However, we observe that the Widmanstätten pattern forms even in the lowest P-containing IVA iron meteorites (0.02 wt% P; Buchwald 1975), mesosiderites (0.02 wt% P; Jarosewich 1990), pallasites (0.005 wt% P; Buseck et al. 1967), and at least one chondrite (Portales Valley, 0.01 wt% P; Ruzicka 2003). It appears that another phase transformation mechanism must control the formation of the Widmanstätten pattern in low P meteoritic metal.

In this paper, we evaluate four mechanisms that have been proposed to explain the formation of the Widmanstätten pattern in iron meteorites and we propose a new mechanism for low P meteoritic metal. These mechanisms can also be used to explain some of the microstructures developed in the metal of chondrites and stony-iron meteorites.

In the following sections, we use composition data and the respective chemical groups of specific iron meteorites collected by Buchwald in his classical handbook of iron meteorites (Buchwald 1975). Some of the chemical groups have been modified, for example, groups IA, IB, IIIC, and IIID are now called group IAB–IIICD (Choi et al. 1995), groups IIA and IIB are now called group IIAB, and group IIIA and IIIB are now called group IIIAB (Scott and Wasson 1975).

FORMATION MECHANISMS FOR THE WIDMANSTÄTTEN PATTERN IN METEORITES

Mechanism I

Fe-Ni Phase Diagram

The traditional mechanism $\gamma \rightarrow \alpha + \gamma$ for Widmanstätten formation in iron meteorites (Owen and Burns 1939) is based on the binary Fe-Ni phase diagram. This mechanism assumes that α nucleates directly from γ phase within the $\alpha + \gamma$ two-phase region and grows into γ phase as the meteorite cools from high temperature to low temperature (Fig. 1).

Using computer techniques, Wood (1964) and Goldstein and Ogilvie (1965) used mechanism I to simulate the growth of the Widmanstätten structure and obtain cooling rates of meteoritic parent bodies. They did not include the effect of minor amounts of other elements (P, C, S, Co, etc.) on the phase boundaries of the binary Fe-Ni system. These authors found that for some iron meteorites significant under-cooling (100–200 °C) below the $\gamma/(\alpha + \gamma)$ phase boundary was required to match the predicted and measured Ni composition in taenite.

However, there is ample evidence from cooling experiments using Fe-Ni alloys that it is not possible to nucleate α phase directly within single crystal taenite (γ phase) before forming martensite (α_2 phase) (Allen and Earley 1950; Narayan and Goldstein 1984; Reisener and Goldstein 2003a). On the other hand, cooling experiments using Fe-Ni-P alloys (Goldstein and Doan 1972) demonstrated that α phase will nucleate directly within single crystal taenite (γ phase) as a Widmanstätten pattern before forming martensite.

Fe-Ni-P Phase Diagram

The ternary Fe-Ni-P phase diagram, determined by Doan and Goldstein (1970), can be used to show how mechanism I $\gamma \rightarrow \alpha + \gamma$ can be applied in the ternary Fe-Ni-P system. Figure 2 shows isothermal sections of the Fe-Ni-P phase diagram at three different temperatures (850, 650, and 550 °C). Figure 3 shows an iso-Ni concentration section at 8.5 wt% Ni from the Fe-Ni-P phase diagram. We can follow the cooling process for a low P Fe-Ni-P alloy such as alloy "c" or "b" in Figs. 2 and 3.

Moren and Goldstein (1979), Romig and Goldstein (1981a), and Rasmussen et al. (1995) also used mechanism I $\gamma \rightarrow \alpha + \gamma$ to determine the cooling rates of low P IVA irons based on the ternary Fe-Ni-P phase diagram. On cooling from single γ phase, these authors assumed that α nucleates either

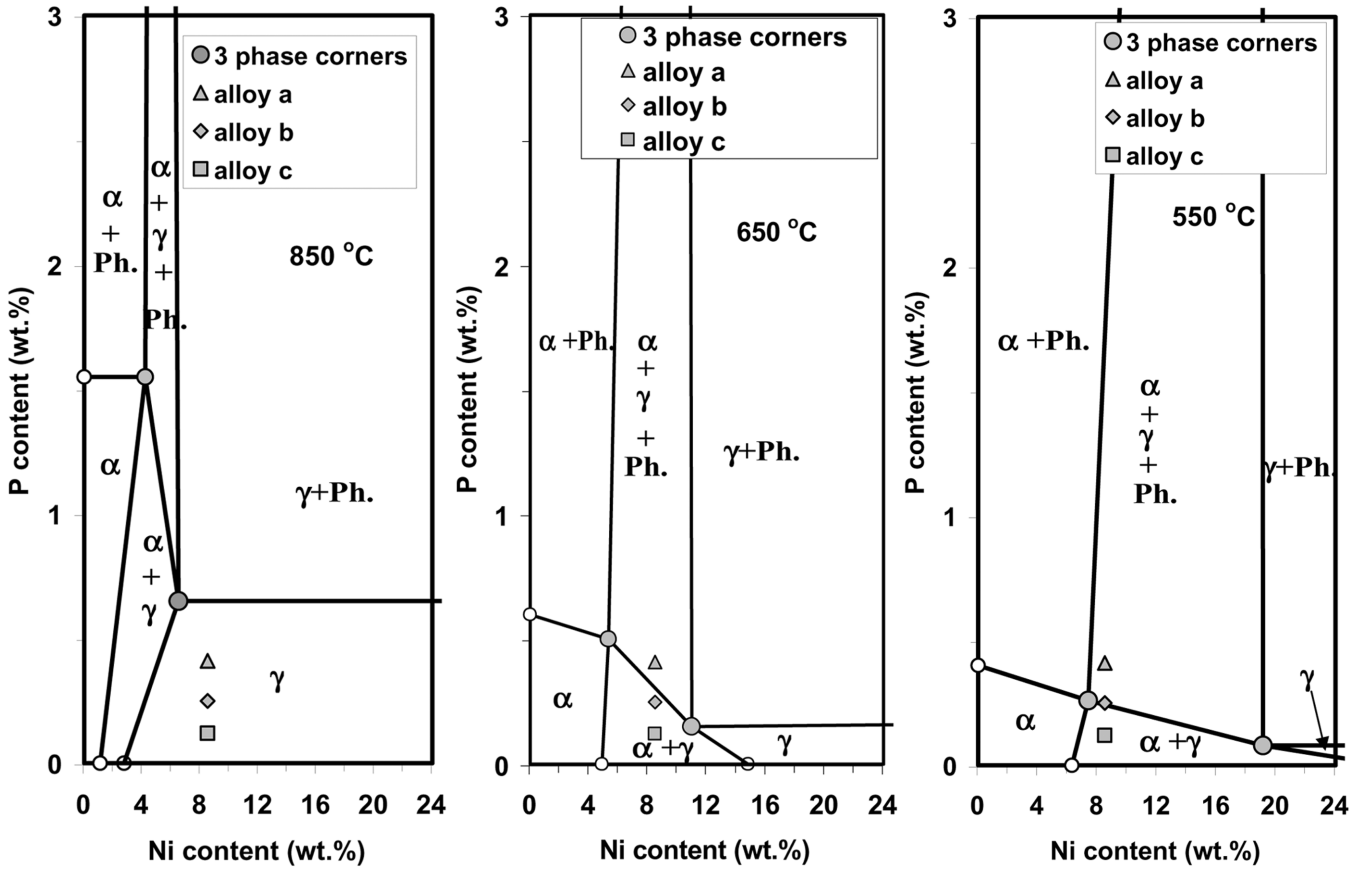

Fig. 2. Isothermal sections of the Fe-Ni-P phase diagram at 850, 650, and 550 °C (open and filled circles are experimental data from Doan and Goldstein 1970). The α and γ corners of the α + γ + Ph three-phase field are shown on the isothermal sections.

at the γ/(α + γ) boundary or in the two-phase α + γ region of the Fe-Ni-P ternary phase diagram. Based on the central Ni versus taenite half width (Wood) method, calculations by Moren and Goldstein (1979) showed that under-cooling of 120–190 °C below the equilibrium γ/(α + γ) phase boundary in Fe-Ni-P phase diagram for α nucleation took place in nine of twelve IVA iron meteorites. The other three IVA irons also required under-cooling. Using the Wood method, Romig and Goldstein (1981a) also applied this reaction path in their cooling rate simulation of the low P IVA iron meteorites. Under-cooling of 65–200 °C was calculated. Mechanism I was also assumed by Rasmussen et al. (1995) in their IVA cooling rate calculation based on the Wood method. They found no under-cooling in low P members of IVA irons and under-cooling of 150–180 °C below the equilibrium γ/(α + γ) phase boundary in the Fe-Ni-P phase diagram for IVA irons with higher P contents.

There are two major problems in applying mechanism I γ → α + γ for low-P-bearing iron meteorites: 1) Narayan and Goldstein (1984) have shown experimentally that α does not nucleate from single crystal taenite in low-P-bearing Fe-Ni alloys. Kamacite cannot nucleate in the two-phase α + γ region of the ternary Fe-Ni-P phase diagram until γ is saturated in P (Figs. 2–3) and 2) the nucleation temperature of α phase is either below the (α + γ)/(α + γ + Ph) boundary or below M_s—the martensite start temperature (Fig. 3) for the low P IVA irons meteorites in which α nucleates after significant under-cooling (Moren and Goldstein 1979; Romig and Goldstein 1981a; Rasmussen et al. 1995). Therefore, mechanism I γ → α + γ is not applicable for the formation of the Widmanstätten pattern. Nucleation of the Widmanstätten pattern either at a temperature below the (α + γ)/(α + γ + Ph) boundary (mechanism III) or by the decomposition of martensite (mechanism V), as discussed in the following sections, is responsible for the formation of kamacite in low-P-bearing meteorites.

Mechanism II

Goldstein and Doan (1972) showed experimentally that the reaction path γ → γ + Ph (phosphide, $[FeNi]_3P$) → α + γ + Ph in ternary Fe-Ni-P alloys can produce a Widmanstätten pattern. The ternary Fe-Ni-P phase diagram (Figs. 2–3) can be used to illustrate this mechanism. On cooling from 850 °C, a high P alloy (such as alloy "a" in Figs. 2–3), phosphide forms first within the γ + Ph phase region (>750 °C). The α phase nucleates from parent γ as the high P alloy cools into the three-phase α + γ + Ph region (~≤700 °C). The α phase grows

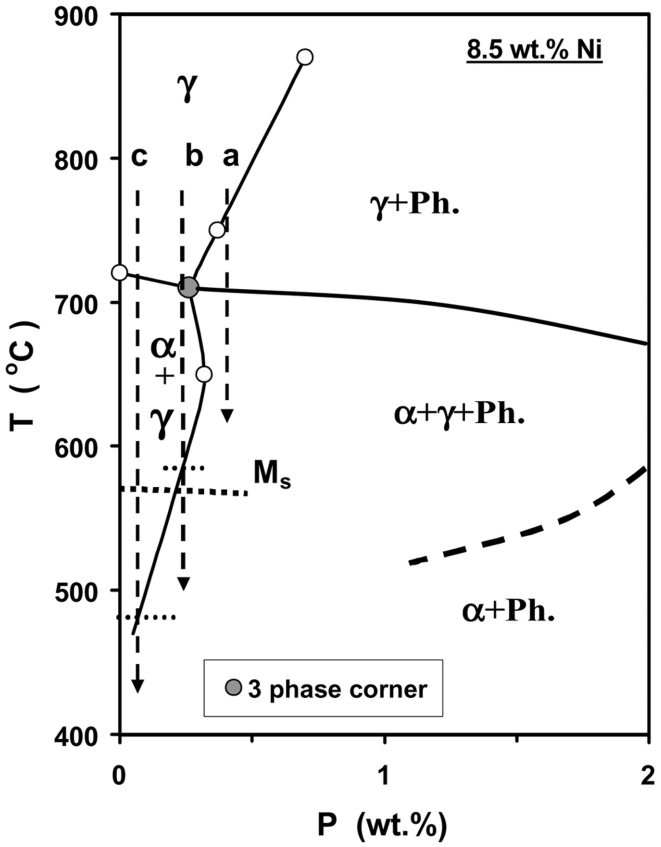

Fig. 3. Iso-Ni concentration section at 8.5 wt% Ni from the Fe-Ni-P phase diagram. M_s represents the martensite start temperature. The vertical dashed lines a, b, and c represent alloys with different P contents cooling from high temperature to low temperature. Alloys a, b, and c form Widmanstätten patterns by mechanisms II, III, and V, respectively. The γ corner of the three-phase α + γ + Ph phase field is shown by the filled circle. The open circles are experimental data from Doan and Goldstein (1970).

into parent γ as the alloy continues to cool. This mechanism has been experimentally observed during cooling of high P Fe-Ni alloys (Goldstein and Doan 1972; Narayan and Goldstein 1984; Reisener and Goldstein 2003a). The nucleation of α phase is dependent on entering the α + γ + Ph phase field. Phosphides must be present in the γ phase. These phosphides may also provide sites for the nucleation of the α phase. The γ – taenite phase, observed in the meteorite microstructure, retains the orientation of the original γ – taenite single crystal. The α – kamacite phase, observed in the meteorite microstructure, forms as a Widmanstätten pattern with an orientation of the close packed {110} bcc planes parallel to the close packed {111} fcc planes of the γ – taenite.

Mechanism II γ → γ + Ph → α + γ + Ph can explain the formation of the Widmanstätten pattern in high P iron meteorites (Goldstein and Doan 1972; Narayan and Goldstein 1985). We define meteorites which enter the three-phase field, α + γ + Ph, via cooling from the γ + Ph field (Fig. 3) as high-P-bearing iron meteorites. The Ni-P region that defines the composition range of high-P-bearing iron meteorites is shown in Fig. 4. Using Ni and P data from Buchwald (1975), the Widmanstätten pattern of iron meteorites from chemical groups IIC, IID, and high P members of IAB–IIICD, IIIAB, IIIE, and IVB forms by mechanism II. Nucleation occurs at the temperature where the meteorite first enters the α + γ + Ph three-phase field. The formation of the Widmanstätten pattern in low P iron meteorites (of groups IAB–IIICD, IIIAB, and IVA) cannot be explained by mechanism II. Low P alloys, such as alloys "b" or "c" (Figs. 2 and 3), do not go through the γ + Ph phase field on cooling before they enter the α + γ + Ph phase field.

Mechanism III

Narayan and Goldstein (1984) determined experimentally that α phase does not nucleate when an alloy is too low in P to enter the three-phase α + γ + Ph field via the γ + Ph phase field (mechanism II, Figs. 3 and 4), and is cooled into the two-phase α + γ field. The α phase nucleates only when γ is saturated in P and enters the α + γ + Ph field. This reaction path is shown for alloys "b" and "c" in Fig. 3. The reaction path γ → (α + γ) → α + γ + Ph is called mechanism III. As in mechanism II, the γ phase observed in the meteorite microstructure retains the orientation of the original γ – taenite single crystal. The α – kamacite phase forms as a Widmanstätten pattern with an orientation of the {110} bcc planes parallel to the {111} close packed planes of the taenite. The designation (α + γ) indicates that the alloy passes through the α + γ two-phase field but kamacite is not formed. Mechanism III is consistent with the results of computer simulations discussed previously in which large amounts of under-cooling comparable with the temperature interval observed between the γ/(α + γ) phase boundary and the (α + γ)/(α + γ + Ph) phase boundary (Fig. 3) were predicted.

For a specific Ni content, the division between low and high-P-bearing meteorites is given by a critical P value (C_P). This critical P value is the P content at the γ corner of the three-phase α + γ + Ph field in the Fe-Ni-P phase diagram (Fig. 2). The critical P value determines whether the γ taenite phase of a meteorite of a given Ni content first enters the γ + Ph field (mechanism II) or enters the α + γ field (mechanism III) on cooling (Figs. 2 and 3). The nucleation temperature for kamacite α is much lower if the P content is less than C_P. For example, Fig. 3 shows that for a meteorite with 8.5 wt% Ni, the kamacite nucleation temperature drops sharply from ~700 °C to ~600 °C as the P content decreases from more than C_P (alloy "a") to slightly less than C_P (alloy "b"). The C_P value as a function of Ni content determines the boundary between high P irons, mechanism II, and low P irons the Widmanstätten pattern of which formed by mechanism III as shown in Fig. 4.

The nucleation temperature for the formation of the Widmanstätten pattern is illustrated using Fig. 5, which

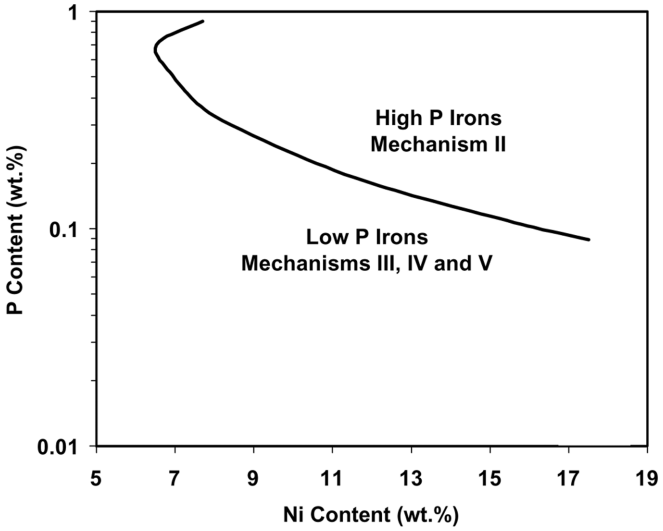

Fig. 4. Ni-P composition ranges for the applicability of mechanism II for high P metal and mechanisms III, IV, and V for low P metal.

shows the binary Fe-Ni and P saturated Fe-Ni-P phase diagrams. The dashed lines on the figure represent the $\gamma/(\alpha + \gamma)$ and the $\alpha/(\alpha + \gamma)$ phase boundaries of the Fe-Ni binary and the solid lines on the figure represent the phase boundaries of the γ and α corners of the three-phase $\alpha + \gamma + Ph$ field in the Fe-Ni-P phase diagram (see Fig. 2). The nucleation temperature of the Widmanstätten pattern formed by mechanism II for high P irons is given by the solid line representing the γ corner of the three-phase $\alpha + \gamma + Ph$ field in the Fe-Ni-P phase diagram. The highest nucleation temperature of kamacite for low P irons based on mechanism III, as a function of Ni content, and illustrated in Fig. 3, occurs at the $(\alpha + \gamma)/(\alpha + \gamma + Ph)$ boundary corresponding to the critical P value (C_P). This temperature is shown by the dotted line plotted on Fig. 5 and is ~70 to 150 °C below the nucleation temperature of the Widmanstätten pattern in high P irons. The Widmanstätten pattern will form at temperatures below the $(\alpha + \gamma)/(\alpha + \gamma + Ph)$ boundary if the P content of the meteorite is less than C_P.

It should be noted that kamacite nucleation cannot occur in the temperature – Ni content region (striped area) between the solid line representing the γ corner of the three-phase Ph field and the dotted line representing the $(\alpha + \gamma)/(\alpha + \gamma + Ph)$ boundary corresponding to the critical P value, C_P. The presence of this temperature – Ni content region (striped region) is consistent with the large amounts of under-cooling, observed by previous authors (Wood 1964; Goldstein and Ogilvie 1965; Moren and Goldstein 1979; Romig and Goldstein 1981a; Rasmussen et al. 1995). Therefore, mechanism III represents a nucleation sequence in which the meteorite passes through the two-phase $\alpha + \gamma$ field but kamacite is not formed. In this situation, the $\gamma \rightarrow \alpha + \gamma$ reaction is suppressed.

There are two problems in applying mechanism III for all the low P iron meteorites. First, the kamacite nucleation

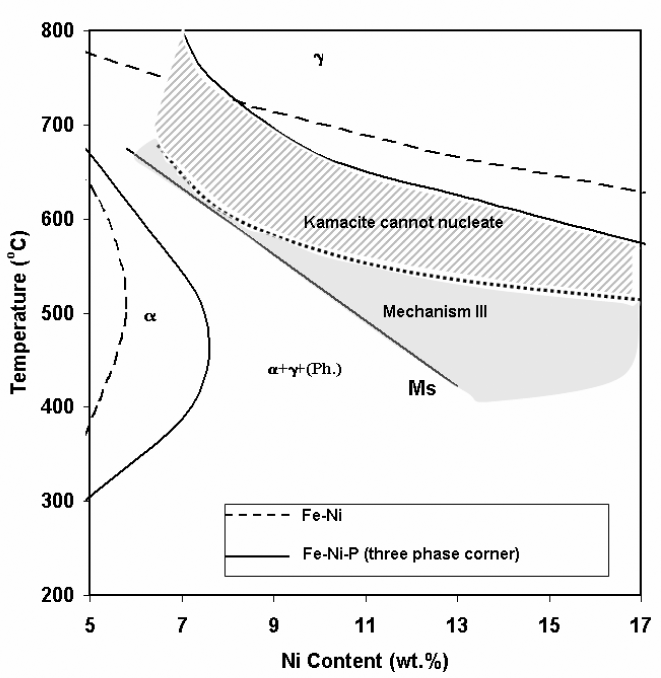

Fig. 5. Nucleation temperatures for the formation of the Widmanstätten pattern in meteoritic metal of varying Ni content. The two dashed lines represent the phase boundaries $\alpha/(\alpha + \gamma)$ and $\gamma/(\alpha + \gamma)$ of the binary Fe-Ni phase diagram. The two solid lines represent the α corner and the γ corner of the three-phase field $\alpha + \gamma + Ph$ in the ternary Fe-Ni-P phase diagram. The M_s line represents the martensite start temperature. The dotted line above M_s represents the upper limit of the application of mechanism III. The shaded zone gives the region in which mechanism III can be applied. The striped zone is the temperature – Ni composition region where kamacite cannot nucleate.

temperature is very low (<500 °C) for meteorites with P contents significantly less than C_P (note Fig. 3). We calculate that a Widmanstätten structure cannot grow to the size observed for the low P meteorites the Widmanstätten pattern of which formed by mechanism III below 500 °C. Therefore, mechanism III cannot be applied to all low P iron meteorites. Second, the nucleation of martensite α_2 will occur when the M_s (martensite start temperature) is higher than the temperature at which a meteorite of a given Ni-P content crosses the $(\alpha + \gamma)/(\alpha + \gamma + Ph)$ boundary. In this case, α_2 forms before the formation of kamacite by mechanism III (note alloy "c" in Fig. 3). When α_2 forms before the $(\alpha + \gamma)/(\alpha + \gamma + Ph)$ phase boundary is reached, α phase nucleation is suppressed.

Because of the two problems in applying mechanism III, we conclude that the temperature – Ni content range in which mechanism III is applicable is restricted to a small temperature – Ni content region given by the shaded region in Fig. 5. For a meteorite of a specific Ni content, the upper temperature limit for the application of mechanism III is determined by the $(\alpha + \gamma)/(\alpha + \gamma + Ph)$ boundary at the critical P value (C_P). The lower temperature limit for the application of mechanism III is determined by the point

where the $(\alpha + \gamma)/(\alpha + \gamma + Ph)$ boundary and M_s intersect. At M_s, α_2 (distorted bcc ferrite) is formed with the same composition as the parent taenite γ phase. The formation of the Widmanstätten pattern in some iron meteorites (i.e., the low P meteorites in chemical group IVB) can be explained by mechanism III. However, the formation of the Widmanstätten pattern in the vast majority of low-P-bearing iron meteorites (as in chemical groups IAB–IIICD, IIIAB, and IVA) is controlled by other mechanisms which involve the formation of martensite α_2.

Mechanism IV

The reaction path $\gamma \rightarrow \alpha_2 \rightarrow \alpha + \gamma$ was proposed as a possible alternative to mechanism I $\gamma \rightarrow \alpha + \gamma$ for the formation of the Widmanstätten pattern for iron meteorites by Owen (1940) and Buchwald (1966). This reaction path is called mechanism IV. Owen (1940) proposed that high temperature γ phase is transformed into metastable α_2, which on reheating at comparatively low temperature transforms into a mixture of α and γ phases. Similarly, Buchwald (1966) postulated that typical Widmanstätten structures result from a two-step reaction: a) $\gamma \rightarrow \alpha_2$ where martensitic forms, followed by b) $\alpha_2 \rightarrow \alpha + \gamma$, where α_2 decomposes at low temperature to $\alpha + \gamma$. In this transformation scheme, γ precipitates from α_2, and the remaining α_2 (which is distorted bcc structure) transforms to α. Both Owen (1940) and Buchwald (1966) imply that γ fully transforms to α_2 and that kamacite and taenite in the Widmanstätten pattern are the result of the decomposition of α_2.

A schematic of mechanism IV, proposed by Owen (1940) and Buchwald (1966), is shown in Fig. 6a. The left-side of Fig. 6a shows the development of the micro-structure of the metal during cooling from the initial taenite phase and the right-side of Fig. 6a shows the evolution of the Ni profile during cooling. T_1 indicates a temperature above M_s, where the metal is one-phase taenite. At temperature T_2 (which is M_s) taenite starts to transform to martensite α_2, which has the same Ni content as taenite. The α_2 is crystallographically related to the parent γ – taenite by the Kurdjumov-Sachs (K-S) or the Nishiyama-Wasserman (N-W) relations. Both crystallographic relations match the close packed planes of the fcc (taenite) and bcc (martensite – α_2) structures of $\{111\}_\gamma // \{110\}_\alpha$. There are four independent choices of the $\{111\}_\gamma$ plane which leads to the classic Widmanstätten pattern for martensite – α_2.

With further cooling to temperature T_3 (which is below M_s) more taenite transforms to α_2. At T_4 (called M_f) all the taenite is transformed to α_2 and the Ni composition in α_2 is the same as the bulk Ni content of original taenite. At temperature T_5, α_2 decomposes, and taenite γ nucleates and grows from the α_2. The γ phase will have a crystallographic relationship to the parent martensite – α_2 by the K-S or N-W relations. The γ – taenite phase (which forms on cooling below T_5) will have different crystallographic orientations than the parent taenite phase.

Because the initial Ni content of the taenite (formed at T_5) is determined by the $\gamma/(\alpha + \gamma)$ equilibrium phase boundary, the initial Ni content of the taenite is much higher than the bulk Ni content of the metal. At the same time, the α_2 phase next to the taenite transforms to α phase with an equilibrium Ni composition given by the $\alpha/(\alpha + \gamma)$ phase boundary (Fig. 1). The taenite γ will continue to grow upon cooling until temperature T_6, where all the remaining α_2 is transformed to kamacite α. The α has a lower Ni content than the bulk Ni of the metal (see Fig. 6a). Although the Ni content in taenite continues to increase due to diffusion, the equilibrium Ni content can only be maintained at the α/γ interface. A Ni gradient develops in taenite due to slow diffusion in taenite with decreasing temperature. As cooling continues and approaches temperature T_7 (which is below 300 °C) the α/γ interface composition continues to change according to the $\alpha/(\alpha + \gamma)$ and $\gamma/(\alpha + \gamma)$ phase boundaries (Fig. 1). Finally, a typical M profile developed. It should be noted that during cooling from T_5 to T_7 taenite will grow to a maximum width and then shrink, dictated by the lever law (Fig. 1). It appears that the two-step reaction mechanism: a) $\gamma \rightarrow \alpha_2$ and b) $\alpha_2 \rightarrow \alpha + \gamma$, may explain the formation of the Widmanstätten pattern in low P iron meteorites where the kamacite nucleation temperature falls below M_s.

Computer simulation studies, based on mechanism IV for mesosiderites (Hopfe and Goldstein 2000) and for low P IVA irons (Goldstein and Hopfe 2001), showed that mechanism IV may be a viable mechanism for the formation of the Widmanstätten pattern in low P meteoritic metal. There is, however, a problem with the two-step mechanism IV as shown by the measured Ni profiles in some low P iron meteorites (Short and Andersen 1965; Massalski et al. 1966). Figure 7 shows that the minimum Ni content in the retained taenite of two low P irons, Sacramento Mountains (IIIAB) and Bristol (IVA), is close to the bulk Ni content of the iron meteorite. Several additional examples of low P iron meteorites such as Duchesne (IVA) and Altonah (IVA) also show that the taenite central Ni content is almost same as the bulk Ni of their respective iron meteorite (Wood 1964; Short and Andersen 1965). If one applies the two-step reaction mechanism IV $\gamma \rightarrow \alpha_2 \rightarrow \alpha + \gamma$ to explain the formation of the Widmanstätten pattern in low P iron meteorites, for example, Bristol (8.07 wt% Ni, 0.06 wt% P), the initial Ni content in the γ phase which nucleates from α_2 at ~600 °C (see T_5 in Fig. 6a) will be ~20 wt%. This Ni content is much higher than the bulk Ni content of the meteorite (8.07 wt% Ni). Since the Ni content in γ phase will continue to increase with decreasing temperature (Fig. 6a), it is impossible for the taenite central Ni content to be the same as the bulk Ni content (Fig. 7). Based on the above discussion, the two-step reaction mechanism IV $\gamma \rightarrow \alpha_2 \rightarrow \alpha + \gamma$ cannot be applied to the formation of the Widmanstätten pattern in low P iron meteorites.

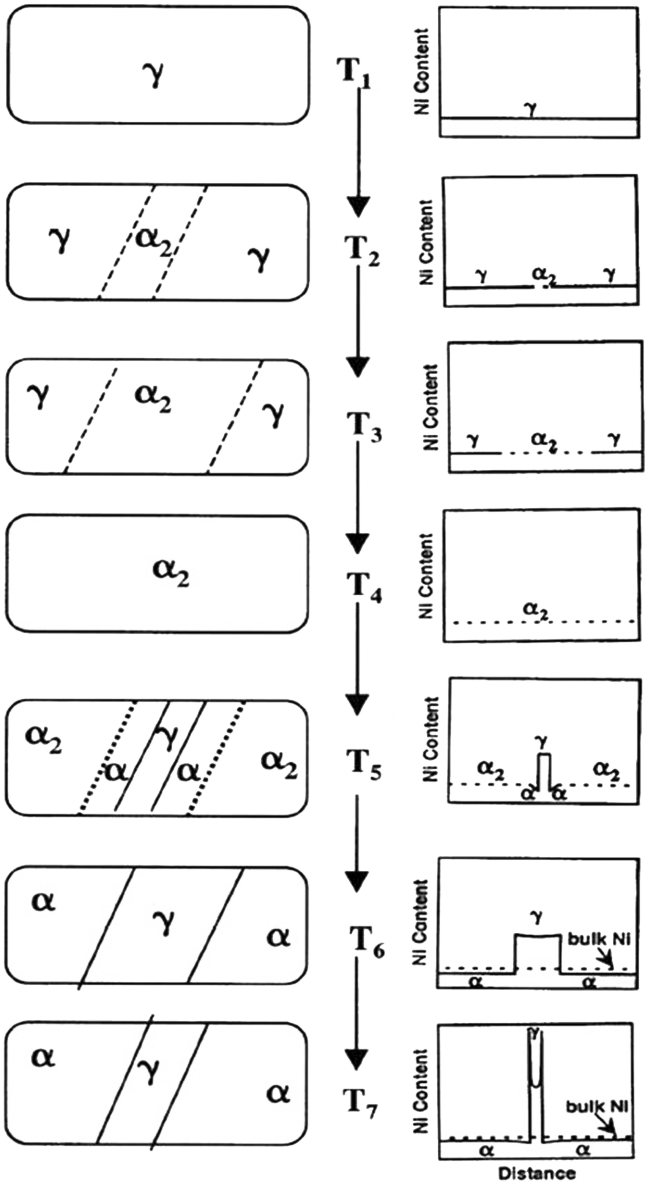

Fig. 6a. Schematic of the formation of the Widmanstätten structure based on mechanism IV $\gamma \rightarrow \alpha_2 \rightarrow \alpha + \gamma$ in meteoritic Fe-Ni alloys. The left-side of the figure shows the development of the microstructure and the right-side shows the development of the Ni profiles in taenite and kamacite as an alloy cools. T_1 through T_7 represent different temperatures during cooling.

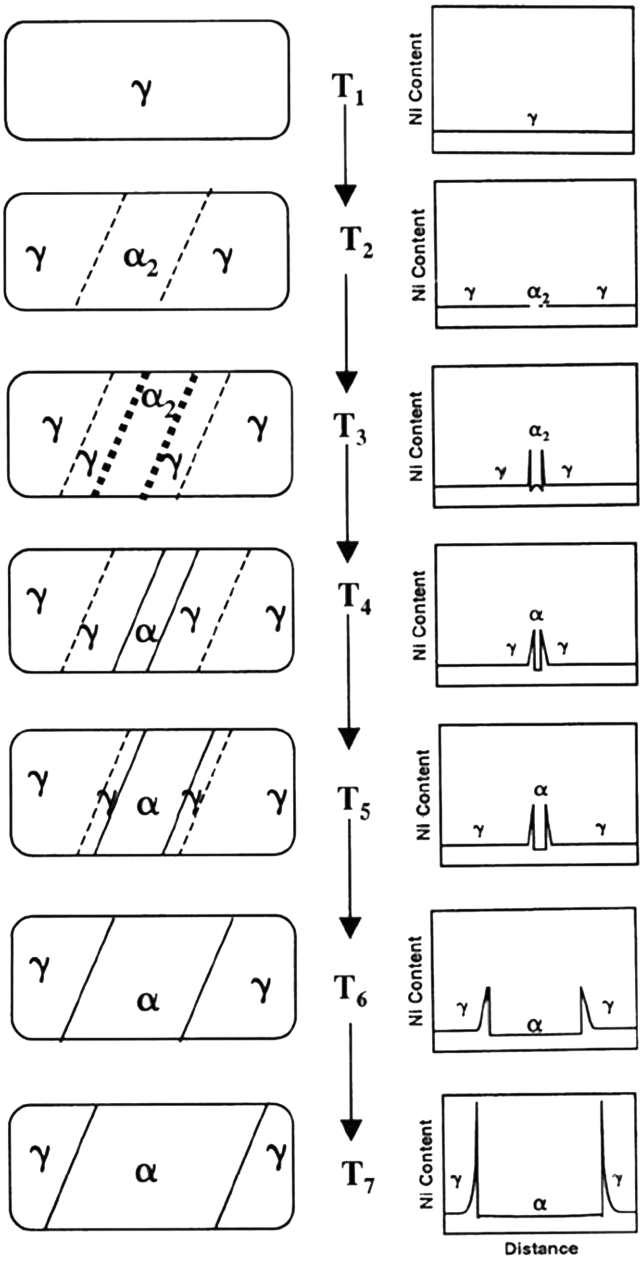

Fig. 6b. Schematic of the formation of the Widmanstätten structure based on mechanism V $\gamma \rightarrow \alpha_2 + \gamma \rightarrow \alpha + \gamma$ in meteoritic Fe-Ni alloys. The left-side of the figure shows the development of the microstructure and the right-side shows the Ni profiles in taenite and kamacite which develop as an alloy cools. T_1 through T_7 represent different temperatures during cooling.

Mechanism V

Yang and Goldstein (2003a) argued that α_2 does not have to cool to a temperature where γ phase completely transforms to α_2 before α_2 begins to decompose to the Widmanstätten pattern $\alpha + \gamma$. The α_2 phase can transform during cooling by mechanism V $\gamma \rightarrow \alpha_2 + \gamma \rightarrow \alpha + \gamma$. Although mechanism V appears to be similar to mechanism IV, the resultant microstructure and phase transformation process are not the same. A schematic of mechanism V is shown in Fig. 6b. Taenite cools from high temperature to temperature T_1 (which is above M_s). At temperature T_2 (which is M_s) taenite starts to transform to martensite α_2, which has the same Ni content as taenite. The α_2 forms on the close packed planes of fcc γ as given by the K-S or N-W relations. With further cooling to temperature T_3 (which is slightly below M_s) new taenite γ phase nucleates in the α_2 regions. The γ forms epitaxially on the pre-existing untransformed γ phase, which borders the

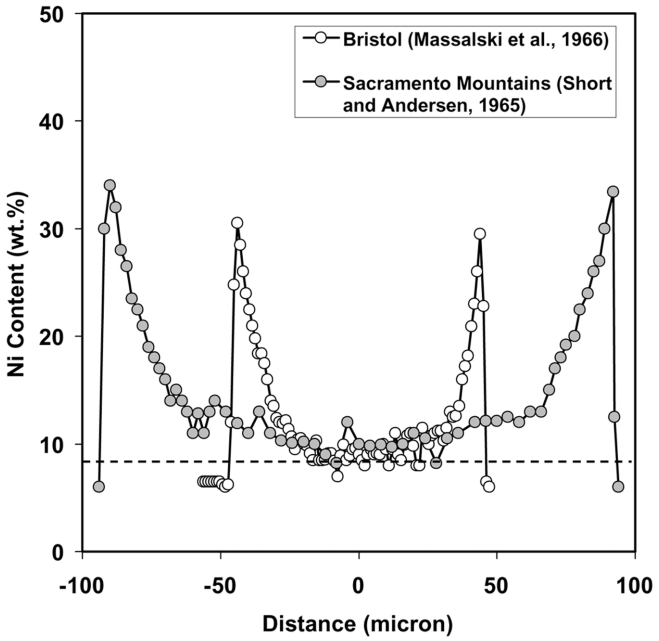

Fig. 7. Measured Ni content profiles in kamacite and taenite in two low P iron meteorites: Sacramento Mountains, IIIAB (Short and Andersen 1965) and Bristol, IVA (Massalski et al. 1966).

martensite α_2 (T_3). The new taenite – γ phase retains the original orientation of the parent taenite (T_1). The Ni content in the new γ phase at T_3 is higher than that in the pre-existing untransformed γ phase. At temperature T_4 (which is slightly below T_3) all the α_2 phase formed at T_2 has transformed into γ and α phases. The α phase which forms has the classic Widmanstätten pattern with specific orientation relationships, (K-S and/or N-W) with the parent taenite. With further cooling to temperature T_5 (which is slightly below T_4) equilibrium is established between the new γ and α phases, and α phase grows into the γ phase. During cooling to temperature T_6, α phase continues to grow into untransformed γ phase and this process continues until the final cooling temperature. At the final cooling temperature, the remaining γ – taenite will have the same crystallographic orientation as the parent γ – taenite at T_1. The α – kamacite of the Widmanstätten pattern will have crystallographic relationships to the γ phase as given by the K-S or N-W relations. At the final cooling temperature (T_7) a typical M profile is produced in the adjacent taenite surrounding the Widmanstätten pattern. Phosphide may form upon further cooling if kamacite or taenite is saturated with P after the α phase forms.

Four factors favor mechanism V over mechanism IV: 1) α_2 is metastable and prefers to decompose into stable α phase on cooling; 2) α_2 decomposes into α and γ grows epitaxially on the parent γ at relatively high temperature (>500 °C); 3) Ni can diffuse more rapidly in both α/α_2 and γ at relatively high temperature (Romig and Goldstein 1981b; Dean and Goldstein 1986; Yang and Goldstein 2004a); and 4) the minimum Ni content of the retained taenite can be the same as the bulk Ni content of the meteorite. Therefore, the Widmanstätten structure in low P iron meteorites forms by mechanism V $\gamma \rightarrow \alpha_2 + \gamma \rightarrow \alpha + \gamma$. This mechanism can explain the formation of the Widmanstätten structure in group IVA, as well as low P IAB–IIICD, IIIAB, and IIIE iron meteorites.

DISCUSSION

Under-Cooling and Kamacite Nucleation Temperatures

Willis and Wasson (1978), Moren and Goldstein (1979), and Romig and Goldstein (1981a) simulated the growth of kamacite (α phase) using the ternary Fe-Ni-P phase diagram and the Wood method to obtain cooling rates of the low P IVA iron meteorites. Willis and Wasson (1978) did not indicate the presence of under-cooling, but their data demonstrate under-cooling at taenite half widths of ≥6 μm. To match the measured Ni data in the taenite phase, Moren and Goldstein (1979) and Romig and Goldstein (1981a) used under-cooling of 65–200 °C below the equilibrium $\gamma/\alpha + \gamma$ phase boundary in the ternary Fe-Ni-P phase diagram (see Fig. 8). The calculated kamacite nucleation temperatures for the formation of the Widmanstätten pattern in the IVA iron meteorites (Moren and Goldstein 1979; Romig and Goldstein 1981a) coincide with M_s, the martensite start temperature (Kaufman and Cohen 1956) (Fig. 8)—the highest temperature at which mechanism V can be applied.

Rasmussen et al. (1995) also simulated the growth of α phase assuming that mechanism I $\gamma \rightarrow \alpha + \gamma$ was responsible for the formation of the Widmanstätten pattern. The authors used the ternary Fe-Ni-P phase diagram and the Wood method and obtained cooling rates of the low P IVA iron meteorites. They argued that kamacite may nucleate in the absence of phosphide. This argument is consistent with mechanism V in which kamacite can nucleate below M_s but above the $(\alpha + \gamma)/(\alpha + \gamma + Ph)$ phase boundary and in the absence of phosphide. In addition, Rasmussen et al. (1995) argued that no under-cooling was necessary for the low P members of the IVA iron meteorites but significant under-cooling (150–200 °C) was necessary for the high P members of the IVA iron meteorites. Unfortunately, central Ni content versus taenite half width data for the low P IVA irons were not given by Rasmussen et al. (1995). Therefore, it is not possible to evaluate the lack of under-cooling asserted for low P IVA irons.

The cooling rate calculation studies of Wood (1964) and Goldstein and Ogilvie (1965) based on the binary Fe-Ni phase diagram, and Moren and Goldstein (1979) and Romig and Goldstein (1981a) based on the ternary Fe-Ni-P phase diagram all use the concept of under-cooling to match the calculated and measured value of Ni in taenite. The nucleation temperature for the formation of the Widmanstätten pattern for each of the three mechanisms (II, III, and V) discussed in this paper is specified by the Ni and

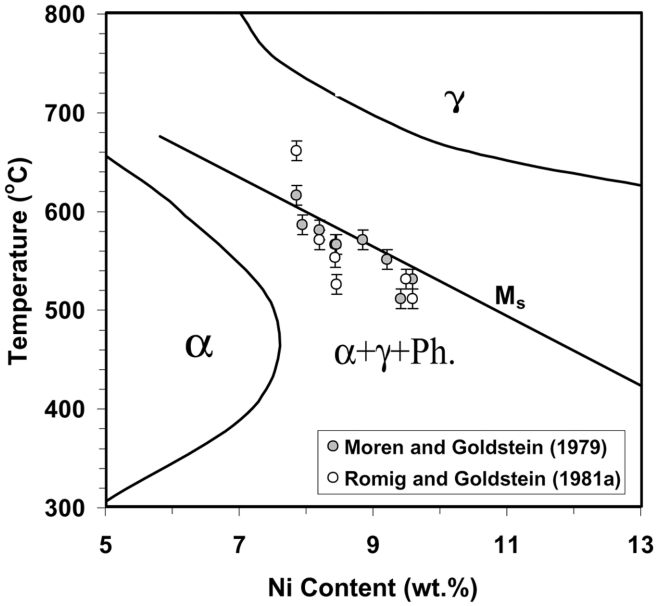

Fig. 8. Kamacite nucleation temperature for IVA iron meteorites (Moren and Goldstein 1979; Romig and Goldstein 1981a) plotted on the Fe-Ni (P saturated) phase diagram. The two solid lines represent the $\alpha/(\alpha + \gamma + Ph)$ corner and the $\gamma/(\alpha + \gamma + Ph)$ corner of the three-phase $\alpha + \gamma + Ph$ field as a function of temperature.

P content of the meteorite. For mechanism II and high P containing meteorites, nucleation occurs at the temperature where the meteorite crosses the $(\gamma + Ph)/(\alpha + \gamma + Ph)$ boundary. For mechanism III and V and for low P containing meteorites, nucleation occurs at the $(\alpha + \gamma)/(\alpha + \gamma + Ph)$ boundary or the M_s temperature, respectively. With the introduction of these three mechanisms, the nucleation temperature is specified. Therefore, there is no need to employ the concept of under-cooling in the calculation of the cooling rate for the formation of the Widmanstätten pattern.

Applicability of Mechanism V: Group IVA

We revised the computer program of Hopfe and Goldstein (2001) to use mechanism V $\gamma \rightarrow \alpha_2 + \gamma \rightarrow \alpha + \gamma$ and determine cooling rates of low P iron meteorites. We have included a modified Fe-Ni equilibrium phase diagram (Yang and Goldstein 2003b) and new interdiffusion coefficients (Yang and Goldstein 2004a) calculated particularly for diffusion below the Curie temperature in kamacite and taenite. Results for the Bristol IVA iron meteorite (8.07 wt% Ni, 0.06 wt% P) are shown in Fig. 9a. A kamacite nucleation temperature (M_s) of 600 °C and a taenite half width of 150 μm are used in the calculation. Preliminary calculations show that there is no apparent difference in choosing various initial α phase sizes (<1 μm) for the calculation. The Ni profile matching method developed by Goldstein and Ogilvie (1965) was used to

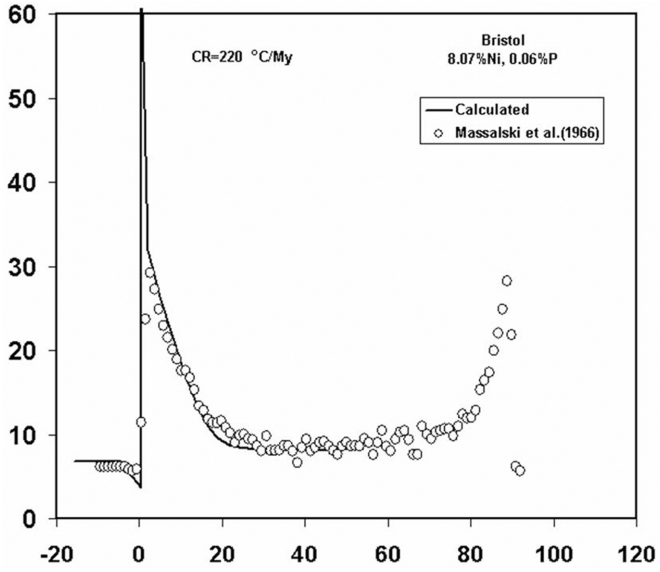

Fig. 9a. Comparison between the measured Ni profile (Massalski et al. 1966) and the calculated Ni profile based on mechanism V for the Bristol IVA iron meteorite.

determine the cooling rate of Bristol iron meteorite. Figure 9a shows that the calculated Ni profile in taenite and kamacite matches the measured Ni profile given by Massalski et al. (1966) when a cooling rate of 220 °C/Myr is used. The cooling rate of 220 °C/Myr is similar to the cooling rate of 150–300 °C/Myr obtained by Saikumar and Goldstein (1988) based on the Wood method (Wood 1964).

We used the revised cooling rate model to determine the cooling rate of a total of 16 IVA irons based on the Wood method (Yang et al. 2004c). The nucleation temperatures for the Widmanstätten pattern in these IVA irons are M_s with a temperature fluctuation within the error limit of M_s obtained by Kaufman and Cohen (1956). Cooling rates vary over an order of magnitude throughout the IVA iron chemical group (Yang et al. 2004c). One of the calculated Wood curves is shown in Fig. 9b for the Duchesne iron meteorite (Yang and Goldstein 2004b). The application of mechanism V gives a good match between the calculated and measured results with a cooling rate of 50–100 °C/Myr. If mechanism II (which is applicable for high P irons) is used, no match is obtained between the calculated and measured results at large taenite half widths (Fig. 9b). Therefore, it is critical to know the formation mechanism for the Widmanstätten pattern to calculate accurate cooling rates.

Criteria for Choosing the Appropriate Widmanstätten Pattern Formation Mechanism

We have observed that for a meteorite of a given Ni content, a critical P content (C_P) separates high P mechanism II from low P mechanisms III and V (Fig 4). For low P irons with P contents below C_P, nucleation of kamacite can occur at

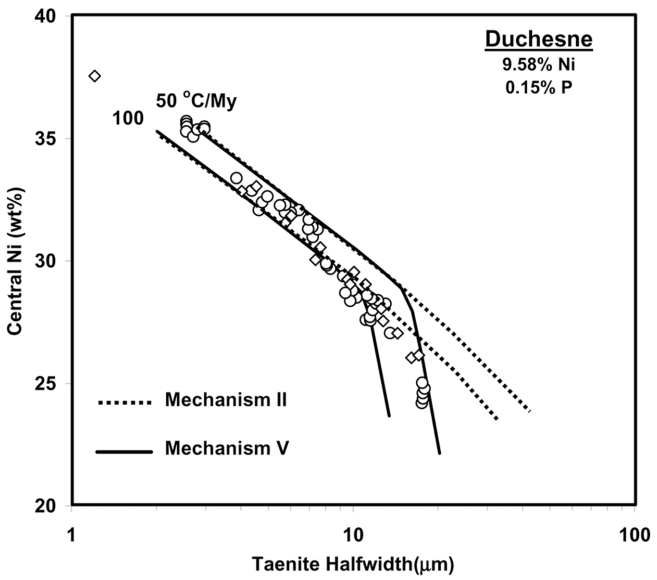

Fig. 9b. Comparison between the measured central Ni versus taenite half width data (open circle, Moren and Goldstein 1979; open diamond, Rasmussen et al. 1995) and the calculated Ni compositions based on mechanism II and V for the Duchesne IVA iron meteorite.

the $(\alpha + \gamma)/(\alpha + \gamma + Ph)$ boundary (mechanism III) or at M_s (mechanism V) (Fig. 3). The specific Ni and P content of the meteorite determines whether the $(\alpha + \gamma)/(\alpha + \gamma + Ph)$ boundary lies above or below the martensite start temperature (M_s) (Fig. 3). Figure 10 shows the Ni-P boundaries for the region of applicability of mechanism II for high P ($>C_P$) irons and of mechanisms III and V for low P ($<C_P$) irons using the Fe-Ni-P phase diagram. The P-Ni region where mechanism III is applicable for the majority of meteoritic metal compositions (7–11 wt% Ni) is very restricted. The restricted temperature – Ni range in which mechanism III is applicable is also shown in Fig. 5.

Widmanstätten Pattern in Iron Meteorites

Bulk Ni and P contents for eight chemical groups of iron meteorites that form a Widmanstätten pattern are plotted in Figs. 10a–10c. Figure 10a shows meteorites in groups IIIAB and IVA. Figure 10b shows meteorites in chemical groups IAB–IIICD, and Figure 10c shows meteorites chemical groups IIC, IID, IIIE, IVB, and IIAB. The Widmanstätten structure in chemical groups IIC, IID, and high P members of groups IIIAB, IAB–IIICD, IIIE, and IVB formed by mechanism II $\gamma \rightarrow \gamma + Ph \rightarrow \alpha + \gamma + Ph$. The Widmanstätten structure in low P members of chemical groups IIAB, IAB–IIICD, IIIAB, IIIE, and IVB iron meteorites formed by mechanism III $\gamma \rightarrow (\alpha + \gamma) \rightarrow \alpha + \gamma + Ph$. The Widmanstätten structure in chemical group IVA and low P members of IAB–IIICD, IIIAB, IIAB, and IIIE formed by mechanism V $\gamma \rightarrow \alpha_2 + \gamma \rightarrow \alpha + \gamma$. For the most populous chemical group (IIIAB) all three mechanisms are applicable while for group IVA irons, for example, only mechanism V $\gamma \rightarrow \alpha_2 + \gamma \rightarrow \alpha + \gamma$ is applicable. As discussed previously, to determine the cooling rate of an individual meteorite in any of the chemical groups of iron meteorites, the appropriate formation mechanism for the Widmanstätten pattern must be established so that an appropriate cooling rate simulation can be applied.

Widmanstätten Pattern in Mesosiderites, Pallasites, and Chondrites

In addition to the iron meteorites, the Widmanstätten structure has been observed in mesosiderites, pallasites, and in at least one chondrite. Information on the P content of these meteorites is not readily available. Metal in mesosiderites contains 7.4–9.4 wt% Ni and 0.02–0.5 wt% P (Buchwald 1975; Jarosewich 1990; Kulpecz and Hewins 1978). Metal in pallasites contains 7.8–16 wt% Ni and 0.005–0.37 wt% P (Scott 1977; Buchwald 1975; Buseck et al. 1967). Widmanstätten pattern metal in the Portales Valley ordinary chondrite contains ~10.7 wt% Ni and ~0.01 wt% P (Ruzicka and Killgore 2002; Ruzicka 2003). As long as the bulk Ni and P compositions in mesosiderites, pallasites, and chondrites are known, the formation mechanism for the Widmanstätten pattern can be determined by one of the three applicable mechanisms (II, III, or V) using the criteria given in this paper (Fig. 10). For example, the Emery mesosiderite contains 9.0 wt% Ni and 0.5 wt% P (Kulpecz and Hewins 1978). If the Ni and P of Emery is plotted in Fig. 10, mechanism II $\gamma \rightarrow \gamma + Ph \rightarrow \alpha + \gamma + Ph$ should be responsible for the formation of the Widmanstätten pattern.

There are a number of meteorites in chemical group IAB–IIICD which contain not only metal with a Widmanstätten pattern but also metal grains in chondritic regions containing microstructures similar to those found in most chondrites (Herpfer et al. 1994). However, the chondrite metal grains contain negligible P. The formation of the zoned taenite microstructure of metal grains in the chondritic regions of these meteorites cannot be explained by any of the three mechanisms (II, III, and V) asserted for Widmanstätten pattern formation. In these chondritic metal regions, the nucleation of α phase occurs at grain boundaries. Kamacite (α phase) will grow into the interior of the taenite grains, as discussed by Reisener and Goldstein (2003a), by mechanism I $\gamma \rightarrow \alpha + \gamma$.

The Portales Valley chondrite is special because it is the only known chondrite which contains not only chondritic metal grains but also metal veins which contain a Widmanstätten pattern. In total, three different micro-structures (Widmanstätten pattern, zoned taenite, and zoneless plessite) are observed in the Portales Valley chondrite (Kring et al. 1999; Reisener and Goldstein 2003b). The metal containing the three different micro-structures in Portales Valley has the same bulk Ni content, is P poor, and has been subjected to the same cooling history. Although

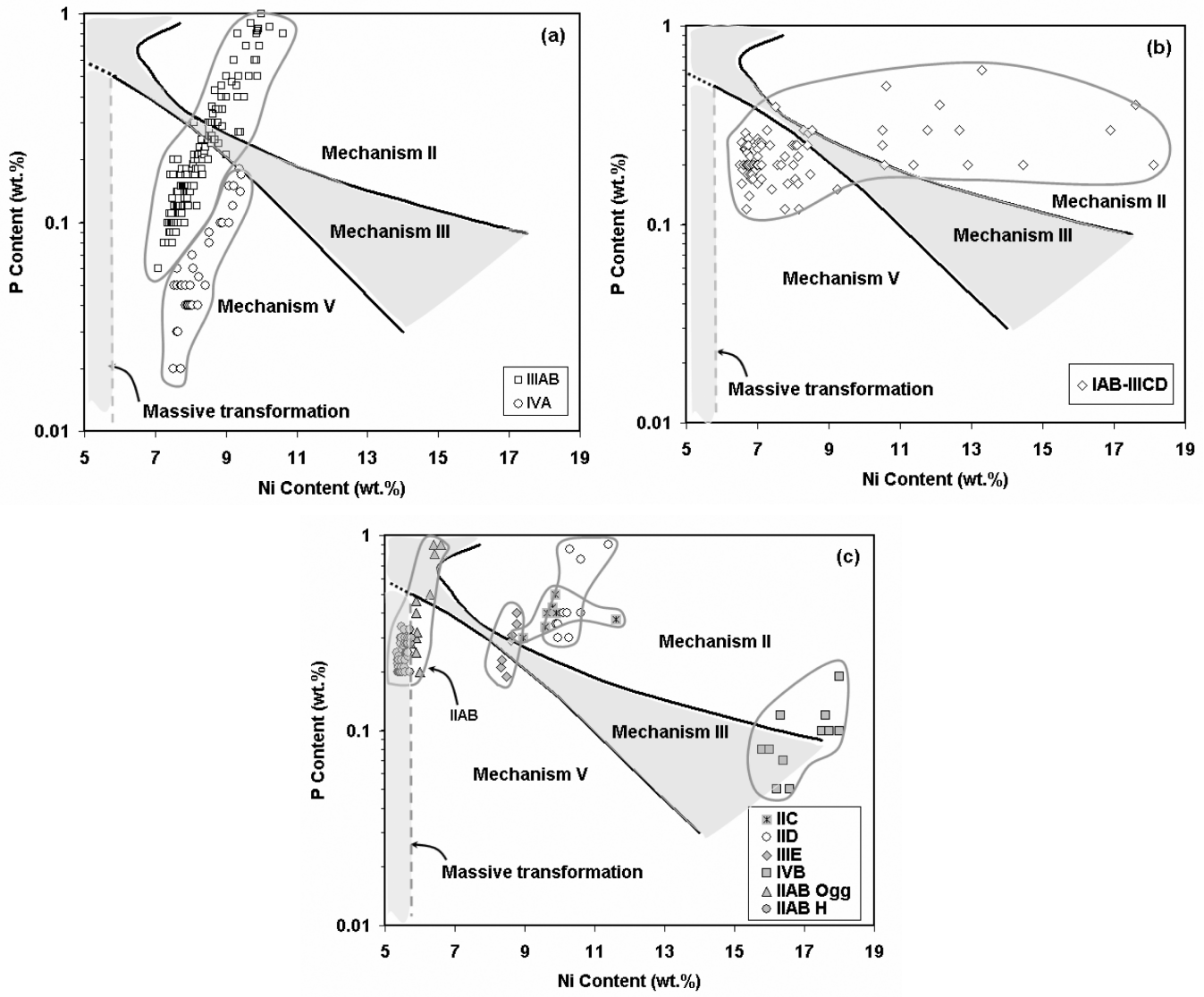

Fig. 10. Dependence of the formation mechanism for the Widmanstätten structure on the Ni and P content of meteoritic metal. Mechanism II represents reaction $\gamma \rightarrow \gamma + Ph \rightarrow \alpha + \gamma + Ph$, mechanism III represents $\gamma \rightarrow (\alpha + \gamma) \rightarrow \alpha + \gamma + Ph$, and mechanism V represents $\gamma \rightarrow \alpha_2 + \gamma \rightarrow \alpha + \gamma$. Groups IIIAB and IVA are plotted in (a), group IAB–IIICD is plotted in (b), and groups IIAB, IIC, IID, IIIE, and IVB are plotted in (c). The massive transformation region which leads to the formation of hexahedrites by the reaction $\gamma \rightarrow \alpha_m \rightarrow \alpha$ in IIAB irons is shown. The estimated boundary between mechanism III and the massive transformation at low Ni contents is given by the dashed line.

coarse phosphate is observed at the margins of some metal veins in Portales Valley (Ruzicka et al. 1999), no phosphide is reported (Scott 2003).

The Widmanstätten pattern is found in large single crystal regions of metal in Portales Valley. Because of the low P content of ~0.01 wt% P (Ruzicka 2003), the Widmanstätten pattern starts to form at M_s (>500 °C) by mechanism V $\gamma \rightarrow \alpha_2 + \gamma \rightarrow \alpha + \gamma$. In the chondritic regions of Portales Valley, both zoned taenite and zoneless plessite are observed. The zoned taenite is formed from small polycrystalline metal grains. Kamacite nucleates and grows at high temperatures along the grain boundaries (Reisener and Goldstein 2003a). The zoned taenite micro-structure is formed by mechanism I $\gamma \rightarrow \alpha + \gamma$. The zoneless plessite microstructure is formed in small isolated single crystals of metal (<100 μm) by mechanism IV $\gamma \rightarrow \alpha_2 \rightarrow \alpha + \gamma$ in which martensite fully develops before the nucleation of kamacite and taenite. The martensite start temperature was probably lower than M_s as measured by Kaufman and Cohen (1956) since small crystals have a lower martensite start temperature than large crystals of the same Ni composition (Kachi et al. 1962; Bando 1964). Kachi et al. (1962) have shown that the decrease in M_s in fine Fe-Ni laboratory alloys results from the decreased number of nucleation sites (dislocations) for martensite formation. In meteoritic Fe-Ni alloys, slow cooling should allow dislocations a much longer time to diffuse out of the interior of the small taenite single

crystals. Therefore, slow cooling should decrease available nucleation sites for martensite formation. It is probable that martensite will form at a lower temperature than M_s as measured by Kaufman and Cohen (1956) (Fig. 1).

Martensite Decomposition: Plessite Structure in Irons, Mesosiderites, Pallasites, and Chondrites

The formation of plessite is dependent on the local Ni content of the γ – taenite and may be promoted by either mechanism IV $\gamma \rightarrow \alpha_2 \rightarrow \alpha + \gamma$ or by mechanism V $\gamma \rightarrow \alpha_2 + \gamma \rightarrow \alpha + \gamma$. For example, duplex plessite forms at the center of the retained taenite and has the same or close to the same composition as the bulk Ni content of the host meteorite (irons, stony-irons, and chondrites). Martensite from which this type of plessite forms is expected to nucleate at relatively high temperature (Fig. 1). As a result, the formation of duplex plessite most likely occurs by mechanism V $\gamma \rightarrow \alpha_2 + \gamma \rightarrow \alpha + \gamma$ in which some of the martensite α_2 decomposes during cooling below M_s. In these low Ni plessite regions, the microstructure can be observed in the optical microscope (Zhang et al. 1993) and often represents a micro-Widmanstätten pattern. In this microstructure, the residual γ phase surrounding α retains the crystallographic orientation of the parent γ – taenite.

Mechanism IV $\gamma \rightarrow \alpha_2 \rightarrow \alpha + \gamma$ most likely is responsible for the formation of the sub-micron scale or fine plessite micro-structure such as black plessite (Zhang et al. 1993) with Ni contents much above the bulk Ni content of the host meteorite in irons, stony-irons, and chondrites. Martensite forms at lower temperatures because of the higher taenite Ni content. In this case, it is more difficult for the newly formed α (by the reaction $\alpha_2 \rightarrow \alpha + \gamma$) to grow into residual γ phase due to sluggish diffusion. Therefore, residual γ phase will continue to transform to α_2 with decreasing temperature (Fig. 6a). In this microstructure, the γ phase that forms does not have the same crystallographic orientation as the parent γ – taenite phase.

For high Ni taenite (~25 wt%) which transforms to α_2 by the reaction $\gamma \rightarrow \alpha_2$ at low temperatures (Fig. 1), further decomposition of $\alpha_2 \rightarrow \alpha + \gamma$ occurs on a very fine scale (Zhang et al. 1993). Therefore, the reaction $\gamma \rightarrow \alpha_2 \rightarrow \alpha + \gamma$ (mechanism IV) is responsible for the formation of the nanoscale decomposed martensite structure in high Ni regions of residual taenite in irons, stony-irons, and chondrites.

Widmanstätten Pattern and the Massive Transformation

We have shown that mechanism V $\gamma \rightarrow \alpha_2 + \gamma \rightarrow \alpha + \gamma$ is responsible for the formation of the Widmanstätten pattern in low P irons. However, a massive phase transformation $\gamma \rightarrow \alpha_m$ can also occur in the two-phase $\alpha + \gamma$ region at a temperature below T_0 (the temperature at which the free energy of metastable γ phase and metastable α phase of the same composition is equal). Both α_2 and α_m are metastable phases with the same composition as the parent γ phase. It is important to consider whether the massive transformation can also lead to the formation of the Widmanstätten pattern.

There are some basic differences between the massive transformation and the martensitic transformation. Speich and Swann (1965), Swanson and Parr (1964), Massalski et al. (1975) and Borgerstam and Hilliert (2000) showed that the border between the massive transformation and the martensitic transformation in binary Fe-Ni alloys lies between 6 and 9 wt% Ni (Fig. 1). The massive transformation is dominant at the low Ni end of the border while the martensite transformation is dominant at high Ni end of the border. At slow cooling rates, the martensitic transformation can also occur in low Ni Fe-Ni alloys, but the massive transformation occurs at higher temperatures than the martensitic transformation (Swanson and Parr 1964). The massive transformation $\gamma \rightarrow \alpha_m$ is an interface-controlled diffusional phase transformation. There are no rational orientation relationships or habit planes between α_m and the parent phase lattice (Massalski 2002). On the other hand, the martensitic transformation is a diffusionless phase transformation in which there are habit and rational orientation relationships between the parent phase taenite and martensite α_2 such as the Kurdjumov-Sachs (K-S) or Nishiyama-Wasserman (N-W) relations.

One of the important features of both the Widmanstätten pattern and the plessite structures in meteoritic metal is that there are rational orientation relationships between the α and γ phases. This observation is consistent with the nature of the martensitic transformation. In addition, the Ni compositions of iron meteorites in all but one of the chemical groups are greater than the lower Ni limit of the border (~6 wt% Ni) between the massive transformation and the martensitic transformation in binary Fe-Ni alloys. Therefore, based on the characteristics of the Widmanstätten pattern and the nature of massive versus martensitic transformations, we argue that the massive transformation cannot lead to the formation of the Widmanstätten pattern or plessite.

Formation of Hexahedrites

The low Ni (5.3–5.75 wt%) members of chemical group IIAB are hexahedrites that have a single crystal structure of kamacite and have the lowest Ni content of all the iron meteorites. Higher Ni (5.75–6.9 wt%) members of group IIAB display a very coarse Widmanstätten pattern with kamacite widths of 5–10 mm. Figure 10c shows the Ni and P content of the members of chemical group IIAB and the corresponding microstructure (hexahedrite H, or very course octahedrite, Ogg). As shown in Fig. 10c, neither mechanism II nor mechanism III is applicable for the formation of hexahedrite structure. Either the martensite transformation $\gamma \rightarrow \alpha_2$ or the massive transformation $\gamma \rightarrow \alpha_m$ may be responsible for the formation of the hexahedrite microstructure.

It is likely that the massive transformation is responsible for the formation of single crystal kamacite (the hexahedrite structure of these IIAB irons) for the following reasons. First, the Ni content of the IIAB irons (5.3–5.75 wt%) with a hexahedrite structure (see Fig. 10c) is less than the low Ni border between the massive transformation and the martensitic transformation in binary Fe-Ni alloys (6–9 wt% Ni). The massive transformation region is shown in Fig. 10. Second, the formation of large kamacite grains is consistent with an important feature of the massive transformation, that is that the massive transformation can lead to large grains or even a single crystal (Perepezko and Massalski 1974, 1975). In fact, kamacite grains in group IIAB hexahedrites are significantly larger (>5 cm) than the kamacite bandwidths of the Widmanstätten pattern of group IIAB irons (0.5–1 cm) with higher Ni and P contents (Buchwald 1975).

For hexahedrites, taenite starts to transform into massive phase α_m at M_a (the massive transformation temperature). This transformation temperature occurs in the two-phase $\alpha + \gamma$ region of the Fe-Ni phase diagram (Fig. 1) and is near the $\alpha/(\alpha + \gamma)$ boundary (Borgenstam and Hillert 2000). The massive phase α_m inherits the composition of the parent γ phase and can grow into a single large crystal. Massive phase α_m becomes a stable α phase with further cooling into the single phase α region. Therefore, the reaction path $\gamma \rightarrow \alpha_m \rightarrow \alpha$ is the probable mechanism for the formation of the low Ni-low P group IIAB hexahedrites. The Ni content of the higher Ni IIAB irons falls just outside the massive transformation range (Fig. 10c). The coarse grained Widmanstätten pattern most likely forms by mechanism III or V depending on the Ni and P content of the meteorite. The large kamacite bandwidths of up to 1 cm are most likely due to the higher nucleation temperature of the kamacite phase (note Fig. 5).

CONCLUSIONS

The Ni and P content of the taenite phase controls the formation of the Widmanstätten structure in meteorites. The kamacite (α phase) nucleates when taenite (γ phase) is saturated in P and enters the $\alpha + \gamma$ + Ph field or when martensite α_2 nucleates at a temperature before γ enters the $\alpha + \gamma$ + Ph field. Three distinct mechanisms are applicable for the formation of the Widmanstätten pattern: mechanism II $\gamma \rightarrow \gamma +$ Ph $\rightarrow \alpha + \gamma$ + Ph, which is applicable to high P taenite; and mechanisms III $\gamma \rightarrow (\alpha + \gamma) \rightarrow \alpha + \gamma +$ Ph and V $\gamma \rightarrow \alpha_2 + \gamma \rightarrow \alpha + \gamma$, which are applicable to low P taenite. The traditional mechanism I $\gamma \rightarrow \alpha + \gamma$, assumed for the formation of the Widmanstätten pattern, is not applicable.

The Widmanstätten structure in iron meteorite chemical groups IIC, IID, and high P members of groups IIIAB, IAB–IIICD, IIIE, and IVB formed by mechanism II. The Widmanstätten pattern in low P members of groups IIAB, IAB–IIICD, IIIAB, IIIE, and IVB iron meteorites formed by mechanism III, and the Widmanstätten pattern in chemical group IVA, and low P members of group IAB–IIICD, IIIAB, IIAB, and IIIE formed by mechanism V. For the most populous chemical group (IIIAB) all three mechanisms are applicable while for chemical group IVA, only mechanism V $\gamma \rightarrow \alpha_2 + \gamma \rightarrow \alpha + \gamma$ is applicable.

To determine the cooling rate of an individual meteorite in any of the chemical groups of iron meteorites, the appropriate formation mechanism for the Widmanstätten pattern must be established first so that an appropriate cooling rate simulation can be applied. The formation mechanism for the Widmanstätten pattern in mesosiderites, pallasites, and chondrites can also be determined by one of the three applicable mechanisms (II, III, or V) as long as the bulk Ni and P compositions of the metal regions are known.

Depending on the Ni and P content of the meteorite, the kamacite nucleation temperature can be determined by either the $(\gamma + \text{Ph})/(\alpha + \gamma + \text{Ph})$ boundary (mechanism II), the $(\alpha + \gamma)/(\alpha + \gamma + \text{Ph})$ boundary (mechanism III), or the M_s temperature (mechanism V). With the introduction of these three mechanisms and the specific phase boundaries where transformations occur, it is no longer necessary to employ the concept of under-cooling in the calculation of the cooling rate for the formation of the Widmanstätten pattern.

We conclude that mechanisms IV $\gamma \rightarrow \alpha_2 \rightarrow \alpha + \gamma$ and V $\gamma \rightarrow \alpha_2 + \gamma \rightarrow \alpha + \gamma$ are responsible for the formation of plessite structures in irons and the metal phases in mesosiderites, chondrites, and pallasites. We propose that the hexahedrites (chemical group IIAB) formed by the massive transformation through the reaction $\gamma \rightarrow \alpha_m \rightarrow \alpha$ at relatively high temperature in the two-phase $\alpha + \gamma$ region of the Fe-Ni-P phase diagram near the $\alpha/(\alpha + \gamma)$ phase boundary.

Acknowledgments–The authors thank Dr. Alex Ruzicka (Portland State University) and Dr. Edward Scott (University of Hawai'i) for information on the P content in the metal veins of Portales Valley chondrite; and Dr. H. Haack, Dr. Edward Scott, and Dr. A. Kracher for providing helpful reviews. The authors acknowledge the financial support from NASA through grant NAG5–11778.

Editorial Handling—Dr. Edward Scott

REFERENCES

Allen N. P. and Earley C. C. 1950. The transformations $\alpha \rightarrow \gamma$ and $\gamma \rightarrow \alpha$ in iron-rich binary iron-nickel alloys. *Journal of the Iron and Steel Institute of Japan* 166:281–288.

Bando Y. 1964. Characteristics of phase transformation in metallic fine particles (martensitic transformation of Fe-Ni alloys and ordering of CuAu and Cu_3Au alloys). *Transactions of the Japan Institute of Metals* 5:135.

Borgenstam A. and Hillert M. 2000. Massive transformation in the Fe-Ni system. *Acta Materialia* 48:2765–2775.

Buseck P. R., Moore C. B., and Goldstein J. I. 1967. Marburg: A new pallasite. *Geochimica et Cosmochimica Acta* 31:1589–1593.

Buchwald V. F. 1966. Iron-nickel-phosphorous system and the

structure of iron meteorites. *Acta Polytechnica Scandinavica* 51: 1–45.

Buchwald V. F. 1975. Handbook of iron meteorites. Their history, distribution, composition, and structure. Los Angeles: University of California Press. pp. 1–1418.

Choi B. G., Quyang X., and Wasson J. T. 1995. Classification and origin of IAB and IIICD iron meteorites. *Geochimica et Cosmochimica Acta* 59:593–612.

Dean D. C. and Goldstein J. I. 1986. Determination of the interdiffusion coefficients in the Fe-Ni and Fe-Ni-P systems below 900 °C (abstract). *Metallurgical Transactions A* 17:1131–1138.

Doan A. S. and Goldstein J. I. 1970. The ternary phase diagram, Fe-Ni-P. *Metallurgical Transactions* 1:1759–1767.

Goldstein J. I. and Ogilvie R. E. 1965. The growth of the Widmanstätten pattern in metallic meteorites. *Geochimica et Cosmochimica Acta* 29:893–920.

Goldstein J. I. and Doan A. S. 1972. The effect of phosphorous on the formation of the Widmanstätten pattern of iron meteorites. *Geochimica et Cosmochimica Acta* 36:51–69.

Goldstein J. I. and Hopfe W. D. 2001. The metallographic cooling rates of IVA iron meteorites (abstract). *Meteoritics & Planetary Science* 36:A67.

Herpfer M. A., Larimer J. W., and Goldstein J. I. 1994. A comparison of metallographic cooling rate methods used in meteorites. *Geochimica et Cosmochimica Acta* 58:1353–1365.

Hopfe W. D. and Goldstein J. I. 2000. The application of metallographic cooling-rate models to mesosiderites (abstract). *Meteoritics & Planetary Science* 35:A77.

Hopfe W. D. and Goldstein J. I. 2001. The metallographic cooling rate method revised: Application to iron meteorites and mesosiderites. *Meteoritics & Planetary Science* 36:135–154.

Jarosewich E. 1990. Chemical analyses of meteorites: A compilation of stony and iron meteorite analyses. *Meteoritics* 25:323–337.

Kaufman L. and Cohen M. 1956. The martensite transformation in the iron-nickel system. *Transactions of the American Institute of Mining and Metallurgical Engineers* 206:1339–1401.

Kachi S., Bando Y., and Higuchi S. 1962. The phase transformation of iron-nickel alloy in fine particles. *Japanese Journal of Applied Physics* 1:307–313.

Kring D. A., Hill D. H., Gleason J. D., Britt D. T., Consolmagno G. J., Farmer M., Wilson S., and Haag R. 1999. Portales Valley: A meteoritic sample of the brecciated and metal-veined floor of an impact crater on an H-chondrite asteroid. *Meteoritics & Planetary Science* 34:663–669.

Kulpecz A. A. and Hewins R. H. 1978. Cooling rate based on Schreiberite growth for the Emery mesosiderite. *Geochimica et Cosmochimica Acta* 42:1495–1500.

Massalski T. B., Park F. R., and Vassamillet L. F. 1966. Speculations about plessite. *Geochimica et Cosmochimica Acta* 30:649–662.

Massalski T. B., Perepezko J. H., and Jaklovsky J. 1975. Microstructural study of massive transformation in Fe-Ni system. *Materials Science and Engineering* 18:193–198.

Massalski T. B. 2002. Massive transformations revisited (abstract). *Metallurgical and Materials Transactions A* 33A:2277–2283.

Moren A. E. and Goldstein J. I. 1979. Cooling rates of group IVA iron meteorites determined from a ternary Fe-Ni-P model. *Earth and Planetary Science Letters* 43:182–196.

Narayan C. and Goldstein J. I. 1984. Nucleation of intragranular ferrite in Fe-Ni-P alloys. *Metallurgical Transactions A* 15:861–865.

Narayan C. and Goldstein J. I. 1985. A major revision of iron meteorite cooling rates: An experimental study of the growth of the Widmanstätten pattern. *Geochimica et Cosmochimica Acta* 49:397–410.

Owen E. A. and Burns B. D. 1939. X-ray study of some meteoric irons. *The Philosophical Magazine* 28:497–512.

Owen E. A. 1940. The structure of meteoritic iron. *The Philosophical Magazine* 29:553–567.

Perepezko J. H. and Massalski T. B. 1974. Beta to zeta massive transformation in Ag-Al alloys. *Journal of Materials Science* 9: 899–910.

Perepezko J. H. and Massalski T. B. 1975. Rapid growth of single-crystals in solid-state utilizing a massive transformation. *Acta Metallurgica* 23:621–631.

Rasmussen K. L., Ulff-Moller F., and Haack H. 1995. The thermal evolution of IVA iron meteorites: Evidence form metallographic cooling rates. *Geochimica et Cosmochimica Acta* 59:3049–3059.

Reisener R. J. and Goldstein J. I. 2003a. Ordinary chondrite metallography: Part 1. Fe-Ni taenite cooling experiments. *Meteoritics & Planetary Science* 38:1669–1678.

Reisener R. J. and Goldstein J. I. 2003b. Ordinary chondrite metallography: Part 2. Formation of zoned and unzoned metal particles in relatively unshocked H, L, and LL chondrites. *Meteoritics & Planetary Science* 38:1679–1696.

Romig A. D. and Goldstein J. I. 1980. Determination of the Fe-Ni and Fe-Ni-P phase diagrams at low temperatures (700 to 300 C). *Metallurgical Transactions A* 11:1151–1159.

Romig A. D. and Goldstein J. I. 1981a. Low temperature phase equilibrium in the Fe-Ni and Fe-Ni-P Systems: Application to the thermal history of metallic phases in meteorites. *Geochimica et Cosmochimica Acta* 45:1187–1197.

Romig A. D. and Goldstein J. I. 1981b. The diffusivity of Ni in Fe-Ni and Fe-Ni-P martensites. *Metallurgical Transactions A* 12: 243–251.

Ruzicka A., Snyder G. A., Prinz M., and Taylor L.A. 1999. Portales valley: A new metal-phosphate-rich meteorite with affinite to netschaevo and H-group chondrites (abstract #1645). 30th Lunar and Planetary Science Conference. CD-ROM.

Ruzicka A. and Killgore M. 2002. Trace-element abundance in the Portales Valley meteorite: Evidence for geochemical fractions (abstract #1918). 33rd Lunar and Planetary Science Conference. CD-ROM.

Saikumar V. and Goldstein J. I. 1988. An evaluation of the methods to determine the cooling rates of iron meteorites. *Geochimica et Cosmochimica Acta* 52:715–726.

Scott E. R. D. and Wasson J. T. 1975. Classification and properties of iron-meteorites. *Reviews of Geophysics* 13:527–546.

Scott E. R. D. 1977. Pallasites-metal composition, classification, and relationships with iron meteorites. *Geochimica et Cosmochimica Acta* 41:349–360.

Short J. M. and Andersen C. A. 1965. Electron microprobe analysis of the Widmanstätten structure of nine iron meteorites. *Journal of Geophysical Research* 70:3745–3759.

Speich G. R. and Swann P. R. 1965. Yield strength and transformation substructure of quenched iron-nickel alloys. *Journal of the Iron and Steel Institute of Japan* 203:480–485.

Swanson W. D. and Parr J. G. 1964. Transformations in iron-nickel alloys. *Journal of the Iron and Steel Institute of Japan* 202:104–106.

Willis J. and Wasson J. T. 1978. Cooling rates of group IVA iron meteorites. *Earth and Planetary Science Letters* 40:141–150.

Wood J. A. 1964. The Cooling rates and parent bodies of several iron meteorites. *Icarus* 3:429–459.

Yang C. W., Williams D. B., and Goldstein J. I. 1996. A revision of the Fe-Ni phase diagram at low temperature. *Journal of Phase Equilibria* 17:522–531.

Yang J. and Goldstein J. I. 2003a. The mechanism for the formation of the Widmanstätten structure in low P iron meteorites (abstract). *Meteoritics & Planetary Science* 38:A33.

Yang J. and Goldstein J. I. 2003b. An improved model to determine the cooling rates of mesosiderites and iron meteorites (abstract #1156). 34th Lunar and Planetary Science Conference. CD-ROM.

Yang J. and Goldstein J. I. 2004a. Magnetic contribution to interdiffusion coefficients in bcc (α) and fcc (γ) Fe-Ni alloys (abstract) *Metallurgical and Materials Transactions A* 35A: 1681–1690.

Yang J. and Goldstein J. I. 2004b. Nucleation of the Widmanstätten pattern in iron meteorites (abstract #1288). 35th Lunar and Planetary Science Conference. CD-ROM.

Yang J., Goldstein J. I., and Scott E. R. D. 2004c. Metallographic cooling rates of IVA iron meteorites revisited (abstract #1347). 36th Lunar and Planetary Science Conference. CD-ROM.

Zhang J., Williams D. B., and Goldstein J. I. 1993. The microstructure and formation of duplex and black plessite in iron meteorites. *Geochimica et Cosmochimica Acta* 57:3725–3735.